Redox Biology 47 (2021) 102156

Contents lists available at ScienceDirect

Redox Biology

journal homepage: www.elsevier.com/locate/redox

Targeting mitochondria-inflammation circle by renal denervation reduces atheroprone endothelial phenotypes and atherosclerosis

Zhuqing Li [a], Qi Li [a], Li Wang [b], Chao Li [b], Mengping Xu [b], Yajun Duan [c,d], Likun Ma [d], Tingting Li [e], Qiao Chen [e], Yilin Wang [e], Yanxin Wang [e], Jiaxin Feng [e], Xuemei Yin [e], Xiaolin Wang [f], Jihong Han [c,f,*], Chengzhi Lu [a,b,**]

[a] School of Medicine, Nankai University, Tianjin, 300071, China
[b] Department of Cardiology, Tianjin First Center Hospital, Tianjin, 300192, China
[c] Key Laboratory of Metabolism and Regulation for Major Diseases of Anhui Higher Education Institutes, Hefei University of Technology, Hefei, 230009, China
[d] Department of Cardiology, The First Affiliated Hospital of the University of Science and Technology of China, Hefei, 230036, China
[e] Department of Cardiology, The First Center Clinical College of Tianjin Medical University, Tianjin, 300070, China
[f] College of Life Sciences, State Key Laboratory of Medicinal Chemical Biology, Key Laboratory of Bioactive Materials of Ministry of Education, Nankai University, Tianjin, 300071, China

ARTICLE INFO

Keywords:
Renal denervation
Endothelial dysfunction
Mitochondrial dysfunction
Inflammation
Atherosclerosis

ABSTRACT

Objective: The disruption of mitochondrial redox homeostasis in endothelial cells (ECs) can cause chronic inflammation, a substantial contributor to the development of atherosclerosis. Chronic sympathetic hyperactivity can enhance oxidative stress to induce endothelial dysfunction. We determined if renal denervation (RDN), the strategy reducing sympathetic tone, can protect ECs by ameliorating mitochondrial reactive oxygen species (ROS)-induced inflammation to reduce atherosclerosis.

Methods and results: ApoE deficient ($ApoE^{-/-}$) mice were conducted RDN or sham operation before 20-week high-fat diet feeding. Atherosclerosis, EC phenotype and mitochondrial morphology were determined. *In vitro*, human arterial ECs were treated with norepinephrine to determine the mechanisms for RDN-inhibited endothelial inflammation. RDN reduced atherosclerosis, EC mitochondrial oxidative stress and inflammation. Mechanistically, the chronic sympathetic hyperactivity increased circulating norepinephrine and mitochondrial monoamine oxidase A (MAO-A) activity. MAO-A activation-impaired mitochondrial homeostasis resulted in ROS accumulation and NF-κB activation, thereby enhancing expression of atherogenic and proinflammatory molecules in ECs. It also suppressed mitochondrial function regulator PGC-1α, with involvement of NF-κB and oxidative stress. Inactivation of MAO-A by RDN disrupted the positive-feedback regulation between mitochondrial dysfunction and inflammation, thereby inhibiting EC atheroprone phenotypic alterations and atherosclerosis.

Conclusions: The interplay between MAO-A-induced mitochondrial oxidative stress and inflammation in ECs is a key driver in atherogenesis, and it can be reduced by RDN.

1. Introduction

Atherosclerosis is a major pathology for coronary artery disease (CAD), the leading cause of death worldwide [1]. Multiple comorbidities, such as hypertension, diabetes mellitus, obesity and aging, have been identified as the risk factors of atherosclerosis. Vascular endothelial dysfunction, characterized by maladaptive alterations in endothelial functional phenotypes, is considered as the initial step in the development of atherosclerosis [2].

Mitochondria is the primary source of reactive oxygen species (ROS) in living cells and a major target of ROS-induced damage [3]. Although mitochondrial dysfunction is a shared pathogenic mechanism for multiple diseases, the role of mitochondria, particularly in endothelial cells (ECs), in the development of atherosclerosis has not been fully investigated. The disruption of mitochondrial redox homeostasis is a pivotal factor in triggering inflammation and stimulating signaling cascades of the innate immune, resulting in endothelial activation and dysfunction

** Corresponding author. Department of Cardiology, Tianjin First Center Hospital, Tianjin, 300192, China.
* Corresponding author. College of Life Sciences, Nankai University, 94 Weijin Road, Tianjin, 300071, China.
E-mail addresses: jihonghan2008@nankai.edu.cn (J. Han), 5020200072@nankai.edu.cn (C. Lu).

https://doi.org/10.1016/j.redox.2021.102156
Received 16 August 2021; Received in revised form 20 September 2021; Accepted 28 September 2021
Available online 29 September 2021

Abbreviations

CAD	coronary artery disease
CAT	catalase
ECs	endothelial cells
GPx4	glutathione peroxidase 4
H2O2	hydrogen peroxide;
HFD	high-fat diet;
IL,	interleukin
IκBα	inhibitor of nuclear factor kappa-Bα
MAO-A/B	monoamine oxidase A or B
MDA	malondialdehyde
NE	norepinephrine;
NF-κB	nuclear factor kappa-B;
Nrf2	nuclear factor E2-related factor 2
PGC-1α	peroxisome-proliferator-activated receptor-γ coactivator-1α
RDN	renal denervation
ROS	reactive oxygen species
SM22α	smooth muscle 22 alpha
SNS	sympathetic nervous system
SOD	superoxide dismutase
Tfam	mitochondrial transcription factor A
TNF-α,	tumor necrosis factor alpha

[4]. Strategies reducing or neutralizing mitochondrial ROS levels may have broad beneficial effects by attenuating inflammatory response, promoting endothelial repair and suppressing atherosclerosis.

Recently, a number of studies have suggested that endothelial dysfunction is often associated with hyperactivity of sympathetic nervous system (SNS) [5–7]. The previous report revealed that arteries are innervated and that neurotransmitters may affect inflammatory leukocyte adhesion to ECs, suggesting SNS is also a factor involved in atherogenesis [8]. However, sympathetic hyperactivity, oxidative stress and inflammation are closely related in unclear manners [9–11].

Monoamine oxidase-A (MAO-A) is a mitochondrial enzyme responsible for metabolism of norepinephrine, the sympathetic neurotransmitter, and generates hydrogen peroxide (H_2O_2) as the by-product of this enzymatic reaction [12]. Interestingly, activation of MAO-A is associated with increased sympathetic drive and elevated norepinephrine spillover. In this process, the excessive H_2O_2 generation leads to mitochondrial oxidative damage, thereby causing vascular injury in the pathology of atherosclerosis [13]. p53 is one of the main effectors of the MAO-A/H_2O_2 axis, and acts as a repressor of peroxisome-proliferator-activated receptor-γ coactivator-1α (PGC-1α) [14], an essential node connecting metabolic regulation, redox control, and inflammatory pathways. These observations, together with the fact that MAO-A is enriched in endothelium, suggest that the persistent activation of MAO-A/H_2O_2 axis in the context of chronic sympathetic hyperactivity can drive mitochondrial ROS-induced inflammatory response in ECs.

Renal denervation (RDN) can effectively reduce systemic sympathetic activity by ablating the sympathetic nerves running through the adventitia of renal artery. It has been used as a novel therapy for resistant hypertension in clinical [15]. In addition, RDN has shown the potential therapeutic effects on insulin resistance, oxidative stress and inflammation [16–18], which are the risk factors of endothelial dysfunction. Our previous study indicated that RDN improves endothelial function in the context of diabetes [19]. Here we set out to determine if RDN can reduce atherosclerosis by improving endothelial function, particularly by the mechanisms associated with the vicious circuit of MAO-A-induced-mitochondrial ROS release and inflammation in ECs.

2. Materials and methods

2.1. Human serum samples

Experiments with human serum samples were approved by the Institute Research Ethics Committee of the First Affiliated Hospital of the University of Science and Technology of China, and were performed in accordance with the principle of the Helsinki Declaration II. After obtaining informed consent, the blood samples were collected from the non-CAD controls (14 males, 6 females, 50–68 years of age) and CAD patients (12 males, 8 females, 51–65 years of age). The detailed inclusion/exclusion criteria and clinical characteristics of non-CAD controls and CAD patients were described in Tables S1 and S2 in the Supplementary Materials.

2.2. Animals

Male ApoE deficient ($ApoE^{-/-}$) mice (8-week-old) were housed at the Animal Center of Nankai University (Tianjin, China) with free access to food and drinking water. After one week of acclimatization, mice were randomly divided into two groups (20 mice/group): the RDN group (RDN) and the sham surgery group (Sham). Mice in RDN group received bilateral RDN surgically and chemically, while mice in Sham group were performed abdominal surgery without RDN. After operations, all mice were fed a pro-atherogenic high-fat diet (HFD) which contains 21% fat and 0.5% cholesterol for 20 weeks. At the end of experiment, mice were anesthetized and euthanized in a CO_2 chamber, followed by collection of blood, renal, renal artery and aorta samples. All of the studies were approved by the Animal Care and Use Committee of Nankai University, and followed the NIH guidelines on the care and use of animals.

2.3. Cell culture and transfection

Human aortic ECs (HAECs, Lonza, USA) were cultured in the Endothelial Basal Medium 2 (EBM-2, Lonza, USA) containing 2% fetal bovine serum (FBS), 50 μg/mL penicillin/streptomycin, and growth factors. Cells at 70–80% confluence were transfected with MAO-A siRNA (Santa Cruz, USA) using Lipofectamine RNAiMAX or PGC-1α CRISPR expression vector (Santa Cruz, USA) using Lipofectamine 2000. After 24 h transfection, cells were switched to EBM-2 medium containing FBS, and received indicated treatment. Human monocytic cell line, THP-1 cells, was purchased from ATCC (Manassas, USA) and cultured in RPMI 1640 medium containing 10% FBS and 50 μg/mL penicillin/streptomycin.

2.4. Renal denervation

After the general anesthesia with isoflurane, mice were placed as a lying position on a platform and opened the abdomen. Renal arteries and veins were identified and all the visible nerves along vessels were severed, then the surface of renal arteries were painted with phenol solution (10% in ethanol) for 5 min using a small brush. The same procedure was applied to another side. In the Sham group, mice were conducted the same procedure except nerves were not severed while renal arteries treated with 0.9% saline instead of phenol solution. The successful RDN was confirmed by determination of renal artery morphology by hematoxylin and eosin (H&E) staining and norepinephrine content in kidney or serum at the end of experiment.

2.5. Determination of atherosclerotic lesions and plaque histology

After collection, mouse entire aorta and 6-μm frozen cross sections of

aortic root were prepared and used to determine *en face* lesions and sinus lesions by Oil red O staining. All the images were obtained with a microscope and used to analyze lesion area (intima) and Oil red O positive area quantitatively by technicians who were blind to the treatment, based on the guidelines for experimental atherosclerosis studies described in the American Heart Association statement [20]. The cross sections of aortic root were also used to determine area of necrotic cores, thickness of fibrosis cap and collagen content by H&E staining and Masson trichrome (Solarbio, China) staining. ROS levels in plaques was determined by dihydroethidium (DHE, Sigma, USA) staining. Apoptotic cells were determined by TUNEL (Vazyme Biotech, China) staining. All images were captured with a Leica DM5000B microscope (Wetzlar, Germany), and conducted quantitative analysis with Image J software.

2.6. Immunohistochemical and immunofluorescent staining

Renal arteries were fixed in 4% paraformaldehyde, embedded in paraffin and prepared 4-μm sections, followed by immunohistochemical staining. Briefly, sections were incubated with anti-tyrosine hydroxylase antibody (Proteintech, 25859-1-AP, 1:200), then with biotinylated goat anti-rabbit IgG. In a blinded manner, the stain intensity (degree of tyrosine hydroxylase staining) was scored as 0, negative; 1, weak; 2, mild; 3, moderate; or 4, strong.

Frozen aortic root cross sections were conducted immunofluorescent staining with primary antibody against CD68 (Santa Cruz, sc-17832, 1:200), SM22α (Proteintech, 10493-1-AP, 1:200), CD31 (Santa Cruz, sc-376764, 1:200), monocyte chemoattractant protein-1 (MCP-1, Proteintech, 66272-1-Ig, 1:200), endothelin-1 (ET-1, Abcam, ab2786, 1:200), vascular cell adhesion molecule-1 (VCAM-1, Proteintech, 66294-1-Ig, 1:200), intercellular adhesion molecule-1 (ICAM-1, Proteintech, 60299-1-Ig, 1:200), TNF-α (Abclonal, A11534, 1:200), IL-1β (Abclonal, A19635,1:200), IL-6 (Abclonal, A14687, 1:200), NF-κB (Santa Cruz, sc-8008, 1:200), or 8-OHdG (Santa Cruz, sc-66036, 1:200), followed by incubation with FITC or rhodamine-conjugated secondary antibody.

HAECs were fixed in 4% paraformaldehyde, permeabilized by 0.5% Triton, blocked with 5% BSA and incubated with primary antibody against NF-κB (Santa Cruz, sc-8008, 1:200), 8-OHdG (Santa Cruz, sc-66036, 1:200), or PGC-1α (Proteintech, 66369-1-Ig, 1:200), followed by incubation with FITC or rhodamine-conjugated secondary antibody.

2.7. Western blot, quantitative real-time PCR, and biochemical and ELISA assay

Total proteins were extracted from mouse tissues or HAECs using the protein lysis buffer containing protease inhibitor (PMSF plus cocktail). An equal amount of total proteins from each sample was used to determine protein expression by Western blot as described [21]. All the Western blot images were scanned and the band density was semi-quantitatively analyzed.

Total RNA extracted from mouse tissues was used to synthesize cDNA using a reverse transcription kit (Invitrogen, USA), followed by quantitative real-time PCR (qPCR) with a SYBR green PCR master mix and the primers with sequences listed in Table S3 in the Supplementary Materials. Expression of mRNA for each gene was normalized by GAPDH mRNA in the corresponding sample.

Mouse serum triglyceride (TG), total cholesterol (TC), low-density lipoprotein cholesterol (LDL-C), high-density lipoprotein cholesterol (HDL-C), apolipoprotein AI (Apo-AI) and Apo-B levels were determined using Mindray Biochemical Analyzer BS-190 (Mindray, Shenzhen, China). Mouse serum free fatty acid (FFA) levels were measured by an enzymatic method (Biolabo, France). The oxidative stress markers including malondialdehyde (MDA) content, superoxide dismutase (SOD) activity, glutathione (GSH) content and total antioxidant capacity (T-AOC) in mouse serum were detected with the corresponding test kits (Solarbio, China).

Levels of norepinephrine (Abnova, China) and MAO-A (Abbexa, UK) in human serum samples, mouse serum cytokines (R&D, USA) and MAO-A levels/activity (Mbbiology, China) were measured by ELISA kits. After transfection and treatment, conditioned medium from HAECs were collected for determination of cytokines (Thermo Scientific, USA) by ELISA kits.

2.8. Transmission electron microscopy

Mouse thoracic aortic tissues were collected after sacrifice, fixed in 2.5% glutaraldehyde and postfixed in 1% osmium teroxide for 2 h. Samples were dehydrated in gradient ethanol solutions by a routine procedure. The ultrathin slices were prepared and viewed with an electron microscope (Hitachi, Japan).

2.9. Measurement of cellular and mitochondrial ROS production

The intracellular ROS production was measured using the dichlorofluorescin diacetate (DCFDA, Solarbio, China) method as described [22]. Briefly, after treatment, cells in 35 mm confocal culture dishes were incubated with DCFDA for 30 min at 37 °C, followed by immediate observation under a confocal microscope (ZEISS, LSM710, Germany) at the excitation/emission wavelength of 480/530 nm.

Production of mitochondrial superoxide in intact cells was measured using MitoSox red fluorescence dye (Invitrogen, USA). After treatment, cells were stained with 1.5 mmol/L MitoSox red and 10 ng/mL Hoechst blue dye (Solarbio, China) for 15 min at 37 °C, followed by washing twice with PBS. The MitoSox fluorescence was measured in random fields with a confocal microscopy (ZEISS, LSM710, Germany). All obtained fluorescence images were analyzed using ImageJ.

2.10. JC-1 staining

Mitochondrial membrane potential was measured using JC-1 dye staining (Solarbio, China). The dye can be accumulated by cell mitochondrion in a mitochondrial membrane potential-dependent manner, and indicated by a fluorescent emission shift from green (Ex/Em: 515/529 nm) to red (Ex/Em: 585/590 nm). The ratio of red fluorescence intensity to green one indicates the state of mitochondrial depolarization, and the decreased ratio refers to mitochondrial dysfunction. Cells were incubated with JC-1 working solution (5 μg/mL) for 30 min at 37 °C and washed twice with JC-1 buffer, followed by observation with a confocal microscopy (ZEISS, LSM710, Germany). All obtained fluorescence images were analyzed using ImageJ.

2.11. Cell viability assay

Cell toxicity indicated as the percentage of cell viability was determined using the standard CCK-8 assay (Solarbio, China). HEACs were seeded in 96-well (1×10^4 cells/well) plates overnight and treated with norepinephrine for 48 h. After treatment, 10 μL CCK-8 solution was added to each well and incubated for 2 h. The absorbance of each well was measured at 450 nm using a microplate reader. Cell viability was normalized to the control group.

2.12. Determination of mitochondrial morphology

Cells were incubated in media containing 20 nmol/L MitoTracker Red CMXRos (Invitrogen, USA) for 30 min at 37 °C, washed with prewarmed PBS. Cells were then observed under a confocal microscope to determine the red fluorescence from MitoTracker Red CMXRos using a 540–552 nm excitation and 590–660 nm emission filter set, and then confocal microscopic images were analyzed with ImageJ software with MiNA program [23].

2.13. Determination of adhesion of monocytes to HAECs

After treatment, HAECs seed in 35 mm confocal culture dishes were added CFSE-labeled THP-1 cells (1×10^5/dish) and co-cultured for 30 min at 37 °C. The none adherent cells were washed away with pre-warmed PBS for 3 times. Cells adhering to HAECs were observed, photographed and counted using ImageJ.

2.14. Statistical analysis

The statistical results for all figures and tables were presented as mean ± SD. GraphPad Prism software (version 7.0, CA) was used for one-way or two-way ANOVA with post hoc Tukey's test or unpaired *t*-test (two-tailed) whenever appropriate, or to calculate Pearson correlation coefficient and the P-value (two tailed). The differences were considered significant at $P < 0.05$.

3. Results

3.1. Norepinephrine and MAO-A are increased associated with atherosclerosis, but reduced by RDN in HFD-fed ApoE$^{-/-}$ mice

The sympathetic hyperactivity is characterized by increased circulating norepinephrine levels [24]. MAO-A is responsible for norepinephrine metabolism and H_2O_2 generation [12]. It remains unclear if increased norepinephrine or MAO-A is associated with the development of atherosclerosis, particularly in CAD patients. Serum samples collected from CAD patients and non-CAD subjects were determined levels of norepinephrine and MAO-A, followed by the correlation analysis. As shown in Fig. 1A and B, compared with non-CAD controls, serum norepinephrine and MAO-A levels were significantly increased in CAD patients. In addition, a strong positive correlation between serum norepinephrine and MAO-A was observed (Fig. 1C), suggesting norepinephrine and MAO-A might be involved in the development of atherosclerosis. Indeed, in the proatherogenic ApoE$^{-/-}$ mice, HFD feeding accelerates the development of atherosclerosis, which was associated with increased norepinephrine and MAO-A levels in mouse serum (Table S4 in the Supplementary Materials).

To test the direct role of inactivation of sympathetic activity on atherosclerosis, the proatherogenic ApoE$^{-/-}$ mice were subjected to RDN operation, followed by HFD feeding for 20 weeks. At the end of experiment, the effect of RDN on structure of renal artery peripheral nerves and norepinephrine production were determined. Compared with the normal nerve architecture in Sham group, the results of H&E staining demonstrate that RDN caused nerve nucleus pyknosis in the renal artery tissue (Fig. 1D). Tyrosine hydroxylase (TH) is one of the indicators of the sympathetic nerve activity and viability. The TH immunohistochemical staining of the renal artery nerves shows RDN significantly reduced TH expression in the tissue (Fig. 1E and F). Thus, RDN clearly ablates the peripheral sympathetic nerves. Correspondingly, RDN substantially reduced norepinephrine levels in circulation and kidney while had slight effect on epinephrine levels (Fig. 1G–J).

The positive correlation between norepinephrine and MAO-A levels in human blood samples, increased norepinephrine levels in HFD-fed ApoE$^{-/-}$ mice which were decreased by RDN (Fig. 1C, G, I; Table S4) indicate RDN may reduce MAO-A expression in HFD-fed ApoE$^{-/-}$ mice. Indeed, compared to Sham group, RDN reduced MAO-A expression in mouse aorta and heart (Fig. 1K; S1B) with little effect on MAO-B expression in mouse aorta (Fig. 1K) and MAO-A expression in mouse liver (Fig. S1A). Correspondingly, RDN decreased MAO-A activity in mouse serum (Fig. 1L). Taken together, the results above suggest the correlation between norepinephrine or MAO-A and the development of atherosclerosis. RDN can decrease norepinephrine and MAO-A levels in proatherogenic mice, which may not only reduce sympathetic hyperactivity, but also play an important role in anti-atherosclerosis.

3.2. RDN reduces atherosclerosis in HFD-fed ApoE$^{-/-}$ mice

The previous studies have demonstrated the controversy effects of RDN on atherosclerosis [25–27]. To further determine the effect of RDN on atherosclerosis and the involved mechanisms, after sham or RDN operation, ApoE$^{-/-}$ mice were subjected to HFD feeding for 20 weeks, a duration can induce lesions substantially. The Oil red O staining on aortas demonstrates that RDN substantially reduced *en face* aortic lesions and sinus lesions in aortic root (Fig. 2A, C).

Necrotic cores formed in the advanced atherosclerotic plaques are initially resulted from accumulated apoptotic macrophage/foam cells, and increases risk of vulnerable plaque rupture and acute atherothrombotic vascular events [28]. Necrotic core area in RDN group was markedly reduced (Fig. 2B), which is consistent with the anti-apoptotic effect of RDN (Fig. S1C). While RDN had little effect on size of fibrous caps or collagen content of atherosclerotic plaques (Fig. 2B, D). Correspondingly, RDN significantly reduced accumulated macrophage/foam cells with little effect on SM22α positive area in lesions (Fig. 2E and F). Taken together, these data suggest that RDN can retard the development of atherosclerosis with reduction of macrophage/foam cell content in plaques.

3.3. RDN improves atheroprone endothelial phenotypes and inflammatory response in HFD-fed ApoE$^{-/-}$ mice

RDN reduced atherosclerosis in HFD-fed ApoE$^{-/-}$mice with no effect on serum lipid profiles, levels of apolipoproteins and free fatty acids (Figs. S2A–G), suggesting RDN is not able to ameliorate hyperlipidemia. Atherosclerosis is also considered as a disease with chronic inflammation of the arterial wall initiated by inflammatory activation of the endothelium [29]. Inflammation-activated ECs can recruit circulating monocytes *via* production of inflammatory cytokines and chemokines, thereby increasing macrophage/foam cell content in plaques. Thus, inhibition of atherosclerosis by RDN might be associated with decreased endothelium inflammation.

To test it, aortic root cross sections were initially conducted co-immunofluorescent staining with anti-CD31 (the marker for ECs) and anti-proinflammatory factor antibodies. Expression of the proinflammatory factors in the endothelium of sinus lesions, such as MCP-1, ET-1, ICAM-1 and VCAM-1, were reduced by RDN (Fig. 3A–D). RDN also reduced expression of inflammatory factors, such as TNF-α, IL-1β and IL-6, in aortic sinus plaques (Fig. 3E–G). Consistently, levels of cytokines, IL-6, IL-1β, TNF-α and CXCL-10, in mouse serum were reduced by RDN (Fig. 3H).

Transcription factor NF-κB, the "master switch" in inflammatory processes, can activate expression of a series of proatherogenic and proinflammatory molecules in ECs. RDN reduced nucleus NF-κB (Fig. 3I) and phosphorylated NF-κB protein (p–NF–κB, the active form of NF-κB) (Fig. S2H) levels in aortic tissue. Meanwhile, expression of inhibitor of nuclear factor kappa-Bα (IκBα) was increased by RDN (Fig. 3J). Taken together, RDN inactivates NF-κB by reducing its expression and nuclear translocation, consequently, it inhibits expression of NF-κB-mediated proinflammatory molecules in aortic ECs.

3.4. RDN reduces vascular oxidative stress to improve mitochondrial functions in HFD-fed ApoE$^{-/-}$ mice

MAO-A-generated H_2O_2 can induce mitochondrial ROS/oxidative stress and mitochondria damage, thereby playing an important role in cardiovascular diseases [30]. Consistent with reduced serum MAO-A activity (Fig. 1L), RDN reduced MAO-A expression in mouse aortas and heart (Fig. 1K; S1B), suggesting RDN may protect ECs against oxidative stress-induced mitochondrial dysfunction.

The ultrastructure of aortic endothelial mitochondria was determined by transmission electron microscopy. In Sham group, mitochondrial enlargement, swelling, hypodense matrix, and vacuolar

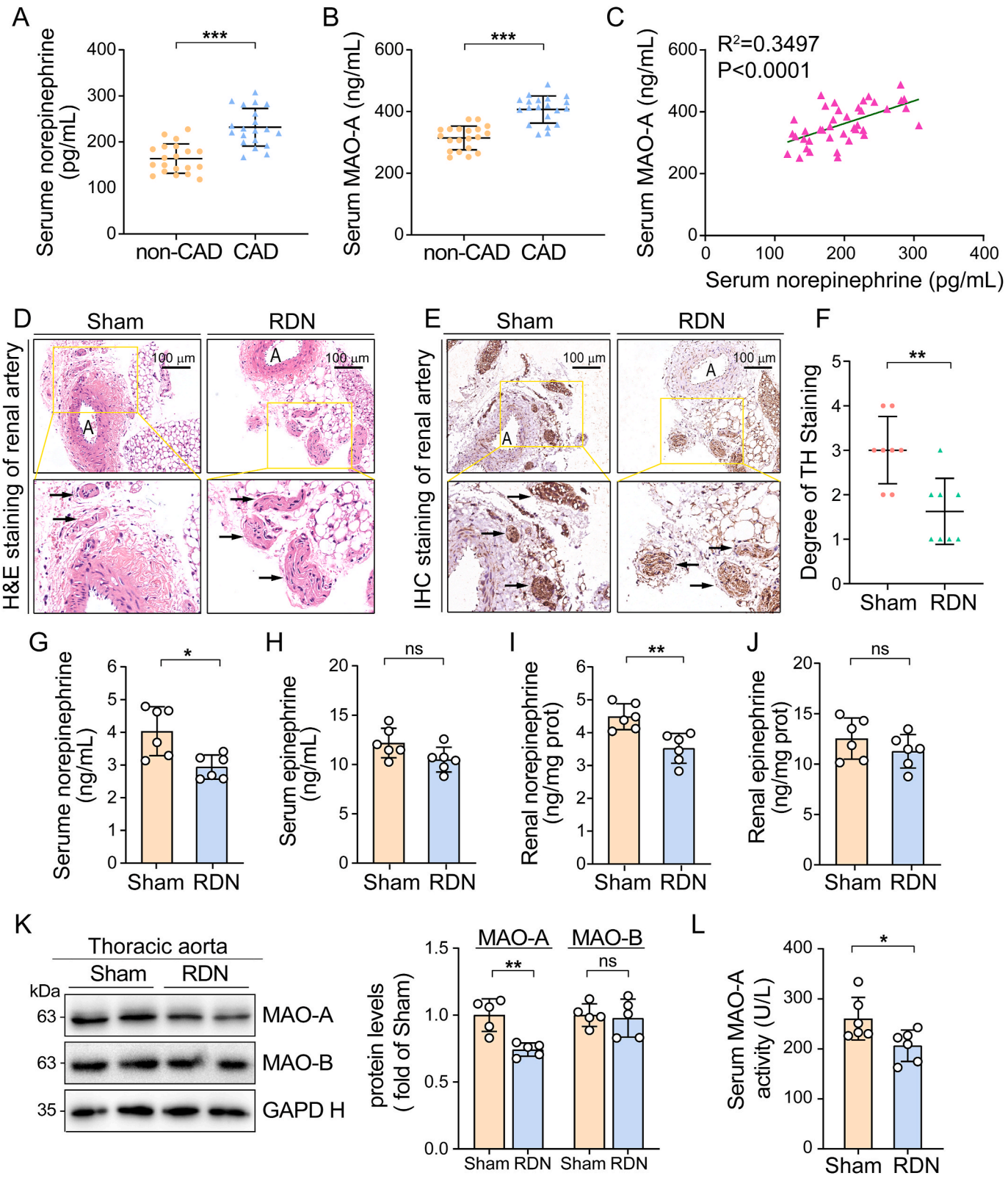

Fig. 1. Increased norepinephrine and MAO-A are observed in CAD patients and reduced by RDN in ApoE$^{-/-}$ miceSerum samples collected from CAD patients and non-CAD controls (n = 20/group) were determined norepinephrine (**A**) and MAO-A (**B**) levels by Elisa assay kits, followed by the correlation analysis between them (**C**). ApoE$^{-/-}$ mice were underwent RDN or sham operation, followed by 20-week HFD feeding (n = 20/group). At the end of experiment, mouse blood, kidney and thoracic aorta samples were collected and used for the following assays. **D, E**: The renal artery sections were conducted H&E staining for structural evaluation and IHC staining for determination of tyrosine hydroxylase (TH) expression. Arrows indicate nerves; A, renal artery. **F**: Degree of TH staining (score): 0, negative; 1, weak; 2, mild; 3, moderate, and 4, strong (n = 8). Serum and kidney lysate were determined norepinephrine (**G, I**) and epinephrine (**H, J**) levels using Elisa kits (n = 6). **K, L**: Expression of MAO-A and MAO-B in thoracic aorta or serum MAO-A activity were determined by Western blot or the assay kit (n = 5). Data are presented as mean ± SD. *P < 0.05; **P < 0.01, ***P < 0.001, ns: not significant.

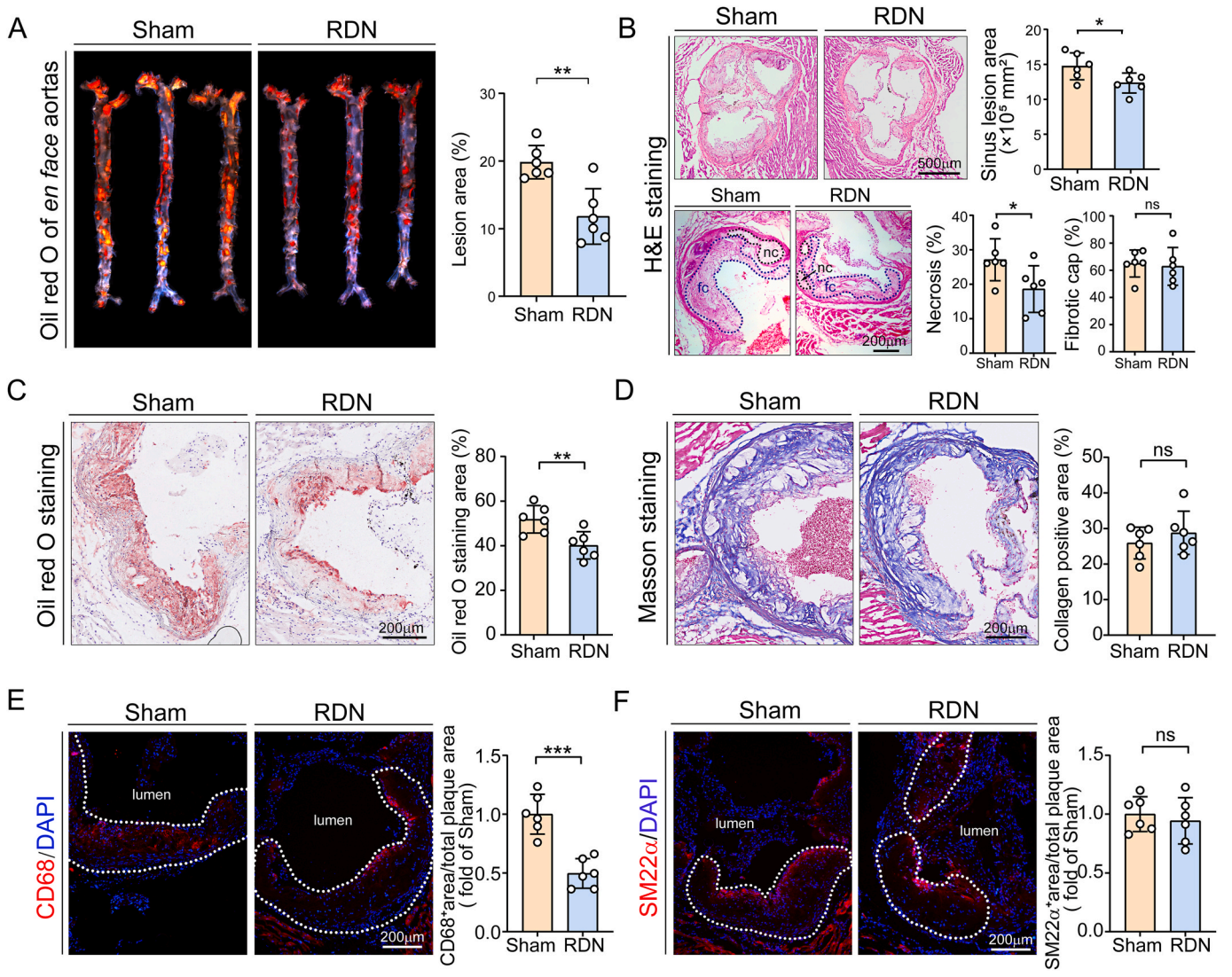

Fig. 2. RDN reduces atherosclerosis in HFD-fed ApoE$^{-/-}$ mice

After sham or RDN operation, ApoE$^{-/-}$ mice were fed HFD for 20 weeks. At the end of experiment, aortas samples were collected and aortic root cross-sections were prepared for the following assays. **A**: Lesions in *en face* aortas were determined by Oil Red O staining and quantified by a computer assisted image analysis protocol (n = 6). **B**: H&E staining followed by quantitative analysis of sinus lesions (upper), necrotic core area and fibrous cap area (bottom) in aortic root cross sections. nc: necrotic cores marked by black dashed lines; fc: fibrous cap marked by blue dashed lines; lesion areas were expressed as μm^2 (n = 6). **C**: Aortic root sections were conducted Oil Red O staining for determination of the percentage of sinus lesions in whole cross-section (n = 6). **D**: Collagen content in arterial wall was determined by Masson trichrome staining with quantitative analysis (n = 6). **E**, **F**: Expression of CD68 (a marker for macrophage) and SM22α (a marker for contractile smooth muscle cell) in aortic root cross-sections were determined by immunofluorescent staining followed by quantification of the fluorescence-positive area in total plaque area (n = 6). Data are presented as mean ± SD. *P < 0.05; **P < 0.01; ns: not significant. (For interpretation of the references to colour in this figure legend, the reader is referred to the Web version of this article.)

degeneration of mitochondrial cristae were observed. In contrast, clear ultrastructure of endothelial mitochondria, dense mitochondrial cristae and matrix with normal density were determined in RDN group (Fig. 4A).

Compared with Sham group, decreased ROS levels in RDN group were determined by DHE staining (Fig. 4B). MAO-A/H_2O_2 axis-induced DNA oxidative damage can be determined by 8OHdG staining. Similar to DHE, aortic endothelial 8OHdG levels were decreased by RDN (Fig. 4C). Correspondingly, levels of oxidative stress indicators in mouse serum, such as SOD, MDA and T-AOC, were markedly decreased, while GSH levels increased significantly by RDN (Fig. 4D–G).

p53 is a main effector of MAO-A/H_2O_2 axis, and acts as a repressor of PGC-1α, a key regulator of mitochondrial biogenesis and antioxidant system in ECs. Thus, a reciprocal expression of p53 and PGC-1α have been reported [14]. Consistently, expression of p53 protein or mRNA in mouse aortas was decreased while PGC-1α expression increased by RDN (Fig. 4H and I). Nuclear factor E2-related factor 2 (Nrf2) is the transcription factor activating expression of several antioxidant molecules [31]. Mitochondrial transcription factor A (Tfam) regulates mitochondrial transcription initiation, DNA packaging, and genome copy number, indicating its critical role in mitochondrial biogenesis [32]. Expression of Nrf2 and Tfam at protein or mRNA levels were significantly increased by RDN (Fig. 4H and I). Correspondingly, expression of antioxidant proteins (SOD2, CAT and GPx4) in aortas were significantly increased by RDN (Fig. 4J). Therefore, these results indicate that RDN can ameliorate mitochondrial oxidative stress by regulating p53/PGC-1α pathway.

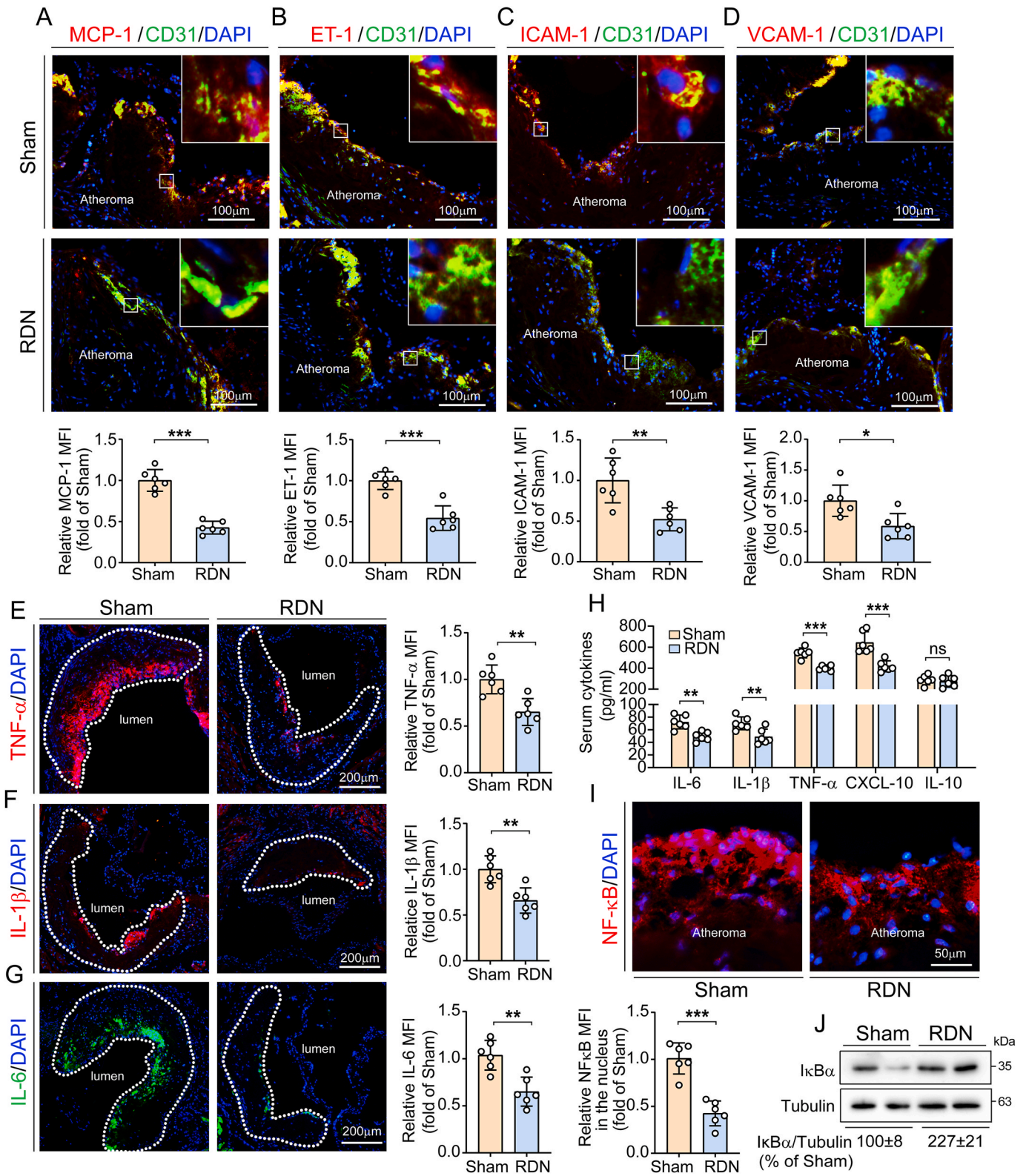

Fig. 3. RDN improves atheroprone endothelial phenotypes and inflammatory response in HFD-fed ApoE$^{-/-}$ mice.
Aortic root cross-sections were conducted co-immunofluorescent staining with anti-CD31 (green) and MCP-1 (red in **A**), ET-1 (red in **B**), ICAM-1 (red in **C**), or VCAM-1 (red in **D**) antibodies (n = 6). The MFI of the indicated molecules in vascular endothelium were quantitatively analyzed. **E-G**: Expression of TNF-α, IL-1β and IL-6 in aortic root cross-section were determined by immunofluorescent staining with quantification of MFI (n = 6). **H:** Serum IL-6, IL-1β, TNF-α, CXCL-10 and IL-10 levels were determined by the corresponding ELISA assay kits (n = 6). **I:** Aortic root cross-sections were conducted immunofluorescent staining with anti–NF–κB p65 antibody with quantitative analysis of MFI in the nucleus (n = 6). **J**: IκBα protein expression in mouse thoracic aorta was determined by Western blot (n = 5). Data are presented as mean ± SD. *P < 0.05; **P < 0.01; ***P < 0.001. ns: not significant. (For interpretation of the references to colour in this figure legend, the reader is referred to the Web version of this article.)

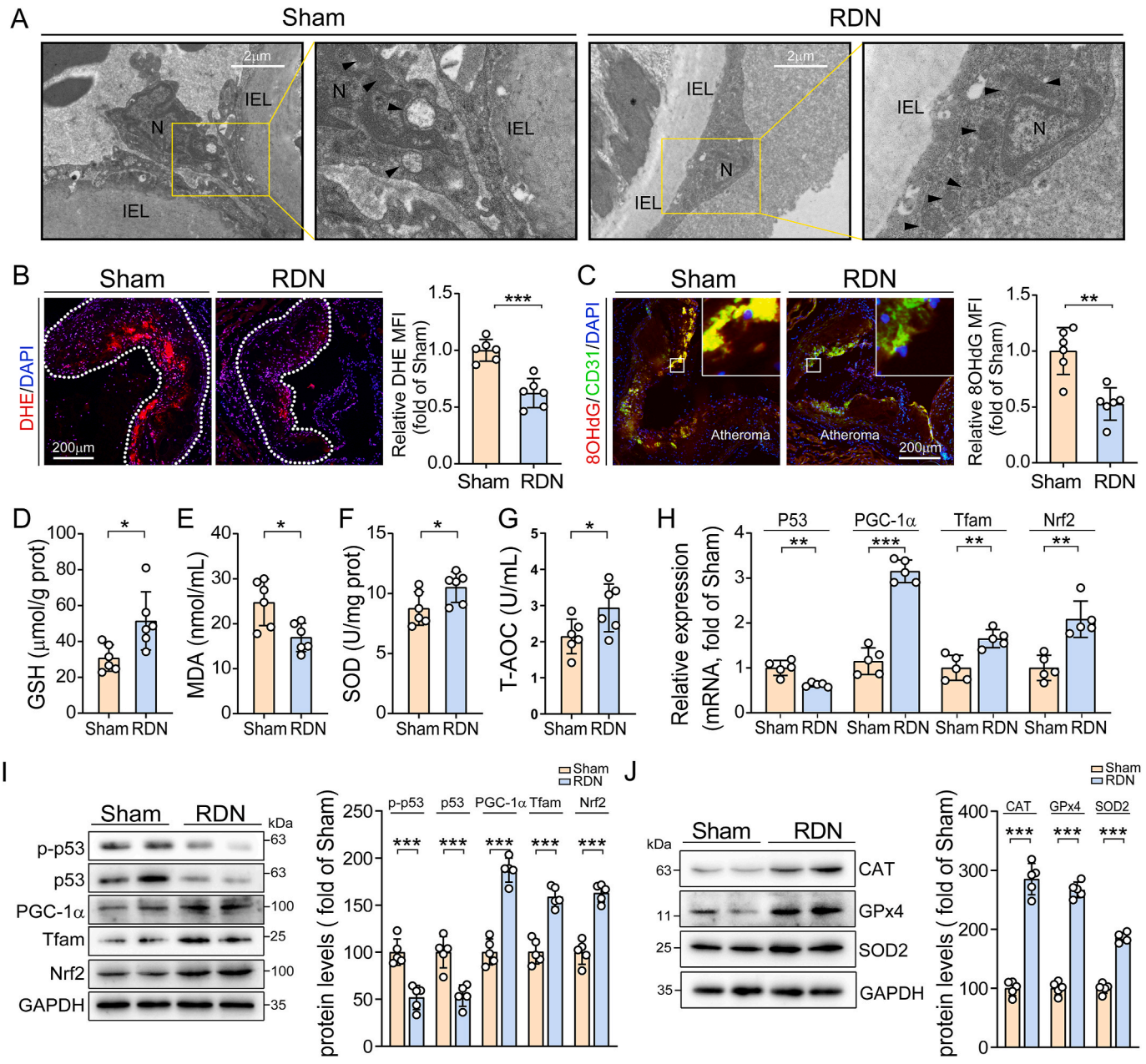

Fig. 4. RDN reduces vascular oxidative stress and improves mitochondrial functions in HFD-fed ApoE$^{-/-}$ mice
A: The ultrastructure of mitochondria in aortic ECs of HFD-fed ApoE$^{-/-}$ mice was observed using a transmission electron microscope (TEM, the original magnification is 40,000). Arrows indicate mitochondria; N, nucleus; IEL, internal elastic laminae. **B**: Aortic root cross-sections were subjected to dihydroethidium staining for determination of the redox state with quantitative analysis of DHE MFI (n = 6). **C**: Arterial tissue sections were conducted co-immunostaining with 8OHdG (red) and anti-CD31 antibody (green) to determine endothelial DNA oxidative stress with quantitative analysis of 8OHdG MFI (n = 6). **D**–**G**: Serum glutathione (GSH) (**D**), malondialdehyde (MDA) (**E**), superoxide dismutase (SOD) (**F**) and total antioxidant capacity (T-AOC) (**G**) levels were determined by the corresponding assay kits (n = 6). **H, I:** Expression of p-p53, p53, PGC-1α, Tfam and Nrf2 mRNA (**H**) or protein (**I**) in thoracic aorta were determined by qRT-PCR or Western blot (n = 5). **J**: Expression of CAT, SOD2 and GPx4 in thoracic aorta were determined by Western blot. Data are presented as mean ± SD. *P < 0.05; **P < 0.01; ***P < 0.001. ns: not significant. (For interpretation of the references to colour in this figure legend, the reader is referred to the Web version of this article.)

3.5. Norepinephrine-activated MAO-A triggers mitochondrial injury and oxidative stress in HAECs

Sympathetic activity is mainly mediated by norepinephrine. Interestingly, cardiovascular risk factors can lead to constantly increased sympathetic tone and circulating norepinephrine [33]. To further determine the interaction between RDN and endothelial function, the effect of norepinephrine on viability of HAECs was initially determined by CCK8 assay. Norepinephrine at low concentrations had little effect on cell viability but significantly reduced it at 100 μmol/L (Fig. S3A), indicating the cytotoxicity of norepinephrine to ECs. Indeed, DCFDA staining shows that norepinephrine increased intracellular ROS levels in HAECs in both concentration and time-dependent manners (Figs. S3B and S3C). Associated with increased ROS production, norepinephrine profoundly changed mitochondrial morphology. The MitoTracker Red staining and analysis on the images with the Mitochondrial Network Analysis (MiNA) toolset demonstrate that mitochondrial footprint and mean branch lengths were significantly reduced by norepinephrine (Fig. 5A).

Although norepinephrine is the substrate for MAO-A activity,

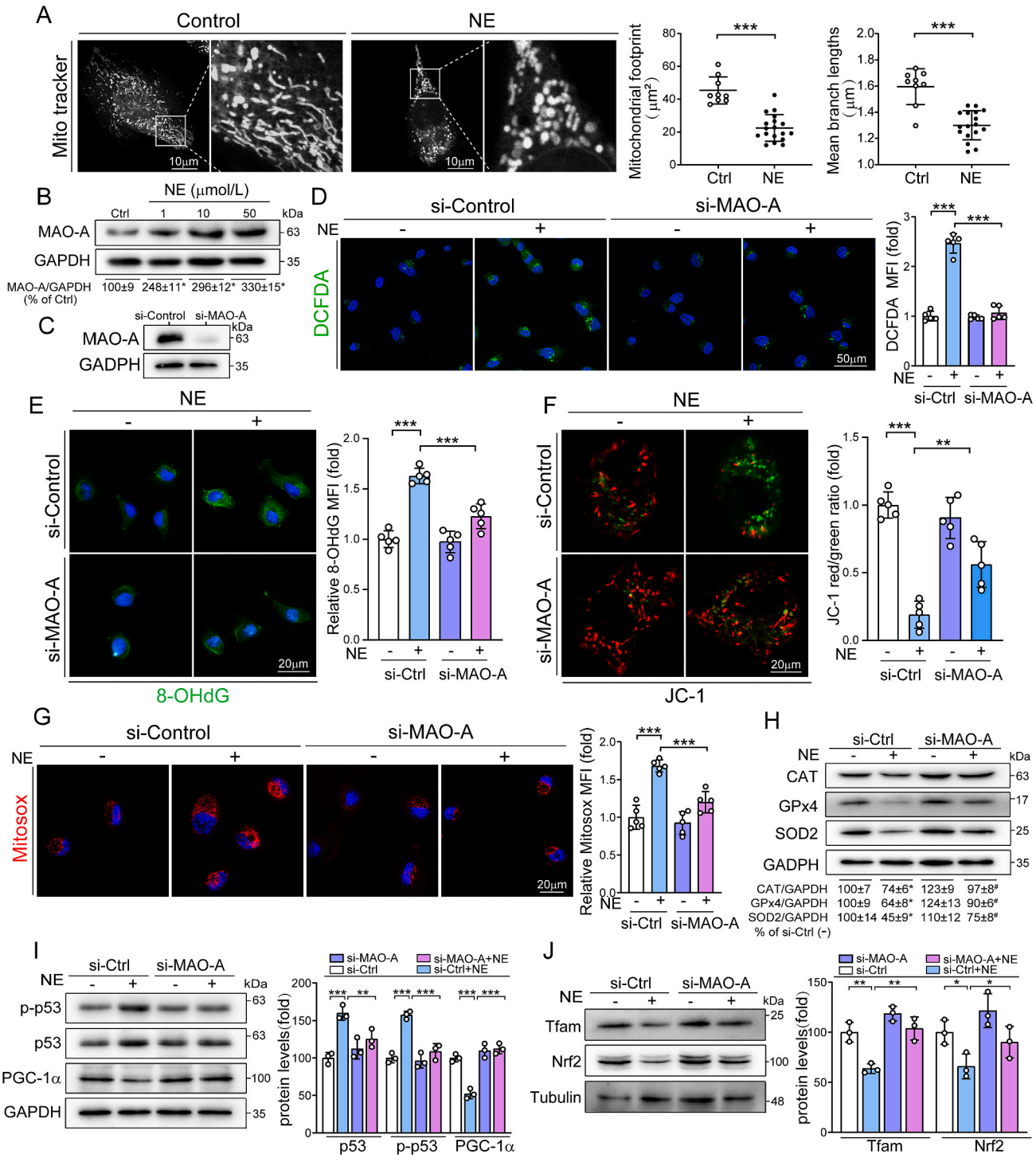

Fig. 5. Norepinephrine-activated MAO-A triggers mitochondrial injury and oxidative stress in HAECs.
A: HAECs were treated with vehicle or norepinephrine (NE, 10 μmol/L) for 24 h, then stained with MitoTracker. After captured, the images were analyzed with MiNA toolset. **B**: HAECs were treated with norepinephrine at the indicated concentrations for 24 h, followed by determination of MAO-A expression by Western blot. **C**: HAECs were transfected with control siRNA (si-Ctrl) or MAO-A siRNA (si-MAO-A) for 24 h, then treated with NE (10 μmol/L) for 24 h, followed by determination of MAO-A protein expression by Western blot. **D**: HAECs were initially transfected with control siRNA (si-Control or si-Ctrl) or MAO-A siRNA (si-MAO-A), then treated with norepinephrine at 10 μmol/L for 24 h. Cellular oxidative stress was determined by DCFDA staining with quantitative analysis of MFI (n = 6). **E–I**: HAECs were transfected with control siRNA or MAO-A siRNA, followed by treatment with norepinephrine (10 μmol/L) for 24 h. Cells were then conducted the following assays. DNA oxidative stress by 8-OHdG staining with MFI quantification (**E**, n = 5). Mitochondrial membrane potential by JC-1 staining with calculation of the ratio of red MFI (aggregated JC-1) to green MFI (monomer JC-1). The ratio in si-Ctrl-transfected alone was defined as 1 (**F**, n = 5). Mitochondrial superoxide levels by MitoSOX Red fluorescent staining with MFI quantification (**G**, n = 5). Expression of CAT, SOD2 and GPx4 (**H**), p-p53, p53 and PGC-1α (**I**), Tfam and Nrf2 (**J**) in HAECs were determined by Western blot. Data are presented as mean ± SD. *P < 0.05; **P < 0.01; ***P < 0.001 *vs.* si-Ctrl without NE treatment or as indicated, #P < 0.05 *vs.* si-Ctrl with NE treatment. ns: not significant. (For interpretation of the references to colour in this figure legend, the reader is referred to the Web version of this article.)

norepinephrine induced MAO-A expression in HAECs in a concentration-dependent manner (Fig. 5B). Interestingly, when MAO-A expression was selectively inhibited by siRNA (Fig. 5C), norepinephrine-induced ROS production and DNA oxidative damage were substantially attenuated (Fig. 5D and E). MAO-A siRNA also significantly improved norepinephrine-impaired mitochondrial functions. Norepinephrine-reduced mitochondrial membrane potential or increased mitochondrial ROS levels were reversed by MAO-A siRNA (Fig. 5F and G).

Cytosolic p53 negatively regulates PGC-1α expression. Associated with increased cytosolic p53 levels in HAECs by norepinephrine, PGC-1α expression was decreased. However, MAO-A siRNA abolished the effect of norepinephrine on p53 and PGC-1α expression (Fig. 5I). Norepinephrine-inhibited expression of mitochondrial biogenesis proteins, Tfam and Nrf2, were also restored by MAO-A siRNA (Fig. 5J). Similarly, expression of antioxidant proteins, CAT, GPx4 and SOD2, were down-regulated by norepinephrine which were attenuated by MAO-A siRNA (Fig. 5H). Taken together, the data above suggest the important role of MAO-A in norepinephrine-induced EC mitochondrial injury and oxidative stress, which is tightly linked to modulation of p53/PGC-1α pathway.

3.6. MAO-A-induced mitochondrial ROS production facilitates expression of NF-κB and atheroprone molecules in HAECs

Activation of mitochondrial ROS production can initiate inflammatory response by activating NF-κB pathway. In HAECs, norepinephrine increased expression of phosphorylated NF-κB while reduced IκBα expression in HAECs (Figs. S3E and S3F; 6A). Consequently, NF-κB nuclear translocation was enhanced by norepinephrine (Fig. 6B; S3D). However, reduced IκBα and increased p–NF–κB or enhanced NF-κB nuclear translocation by norepinephrine were blunted by MAO-A inhibitor, clorgyline (clorg), mitochondrial-targeted anti-oxidant Mito-TEMPO or MAO-A siRNA (Fig. 6A–C; S3D-F).

Both VCAM-1 and ET1 in HAECs were induced by norepinephrine, and the induction was blocked by clorgyline or MitoTEMPO (Fig. 6A). Levels of NF-κB-targeted pro-inflammatory molecules in HAEC conditioned medium, such as MCP-1, IL-6, IL-1β, CXCL-10 and TNF-α, were significantly increased by norepinephrine, and the increases were substantially blocked by clorgyline or MitoTEMPO (Fig. 6C–G). The accumulated macrophage-derived foam cells within artery wall are mainly determined by adhesion of monocytes to endothelium and infiltration. Norepinephrine substantially increased the number of THP-1 cells, a human monocytic cell line, adhering to HAECs, which were blunted by clorgyline and MitoTEMPO (Fig. 6H). These results demonstrate that MAO-A-induced mitochondrial ROS mediates norepinephrine-induced EC proinflammatory and proatherogenic phenotypes by activating expression of NF-κB and its target genes.

3.7. Norepinephrine instigates a positive feedback regulation between PGC-1α and NF-κB

Norepinephrine reduced expression of PGC-1α and mitochondrial biogenetic proteins in MAO-A-dependent manner (Fig. 5H and I). Reciprocally, overexpression of PGC-1α in HAECs (Fig. S4A) not only significantly increased expression of mitochondrial biogenetic proteins, Tfam and Nrf2, and antioxidant molecules, CAT, GPx4 and SOD2, but also blocked the inhibitory effect of norepinephrine on these molecules (Fig. 6I and J). It also inhibited norepinephrine-induced mitochondrial ROS accumulation and mitochondrial DNA oxidation (Fig. 6K; S4B).

PGC-1α and NF-κB mediate each other during inflammation in a vicious circle where the oxidative stress plays a critical role. Transfection of HAECs with PGC-1α expression vector potently attenuated norepinephrine-reduced IκBα and increased NF-κB phosphorylation and nuclear translocation (Fig. 6L; S4E). Associated with NF-κB expression, levels of MCP-1 and IL-6 in HAEC conditioned medium were increased by norepinephrine, and the increases were blocked by PGC-1α-overexpression (Fig. 6M). The adhesion of THP-1 cells to HAECs induced by norepinephrine was also blocked by activation of PGC-1α expression (Fig. S4D). Taken together, the data above suggest that activation of PGC-1α expression can ameliorate norepinephrine-induced mitochondrial oxidative damage by inactivating NF-κB.

4. Discussion

In the current study, we found that RDN ameliorates the sympathetic hyperactivity-induced vicious cycle of EC mitochondrial dysfunction and inflammation, thereby preserving the atheroprotective phenotypes of ECs to inhibit the development of atherosclerosis. Under sympathetic hyperactivity, MAO-A was shown to be a critical regulator of EC functional phenotypes. Persistent MAO-A activation-associated disruption of mitochondrial homeostasis leads to ROS accumulation and NF-κB activation, which activate expression of atherogenic and proinflammatory molecules in ECs. Importantly, the MAO-A/H_2O_2 axis also suppresses the mitochondrial function regulator, PGC-1α, which is mutually regulated by NF-κB during the inflammation in a vicious cycle with essential involvement of oxidative stress. Thus, blockade of MAO-A activation by RDN should be a potential treatment strategy for atherosclerosis.

Sustained sympathetic activation, as indicated by elevated urinary norepinephrine and its metabolite concentrations, efferent muscle sympathetic nerve activity, and increased rates of spillover of norepinephrine to plasma, results in hypertension, diabetes and obesity [34], the risk factors for atherosclerosis. In this study, we found serum norepinephrine levels in CAD patients (Fig. 1A) or HFD-fed ApoE$^{-/-}$ mice (Table S4) were higher than non-CAD controls or normal chow-fed mice, indicating the positive correlation between the development of atherosclerosis and sympathetic hyperactivity. Indeed, a few studies have demonstrated the contradictory effect of RDN on atherosclerosis in animal models with unclear mechanisms [25–27]. The previous published study showed that renal denervation (RDN) can attenuate the development of atherosclerosis in ApoE deficient mice in a blood pressure lowering independent manner [26]. However, another study reported the opposite results that RDN can accelerate the development of atherosclerosis in angiotensin II-induced hypertensive mice [27]. Recently, Chen et al. reported that RDN plays an anti-inflammatory role in atherosclerosis by inhibiting splenic inflammatory cell production [25]. Therefore, based on the contradictory conclusions of the previous studies and the pathogenesis of atherosclerosis, we designed this study to explore the relationship between sympathetic nervous system and atherosclerosis. More importantly, we elucidated the mechanisms based on the function of RDN on endothelial phenotype, particularly in the EC mitochondrial oxidative stress and inflammation. Furthermore, we found that RDN suppressed levels of inflammatory factors, chemokines, and adhesion molecules released by ECs (Fig. 3; 6A-G), thereby inhibiting the adhesion of inflammatory cells to the endothelium (Fig. 6H), which may result in decreased accumulation of macrophage/foam cells in lesion areas (Fig. 2E).

Mitochondrial dysfunction is a strong trigger of endothelial dysfunction in both animal models and humans [36]. Mitochondria play important roles in EC inflammation by regulating ROS production and NF-κB signaling pathway. In this context, the mitochondrial ROS (mtROS)-induced inflammation acts as a feedback system, creating a stressful environment where the exacerbation of inflammation chronically provokes tissue damage [36,37]. In this study, the results of electron microscopy revealed that RDN maintained normal EC mitochondrial morphologies by maintaining mitochondrial membrane integrity and increasing inner mitochondrial cristae (Fig. 4A). In addition, RDN suppressed superoxide generation, DNA oxidative damage and activation of NF-κB pathway, revealing positive antioxidant and anti-inflammatory effects to preserve mitochondrial functions (Fig. 4B–J).

Monoamine oxidase-A is an enzyme located on the outer membranes of the mitochondria. It is responsible for degradation of

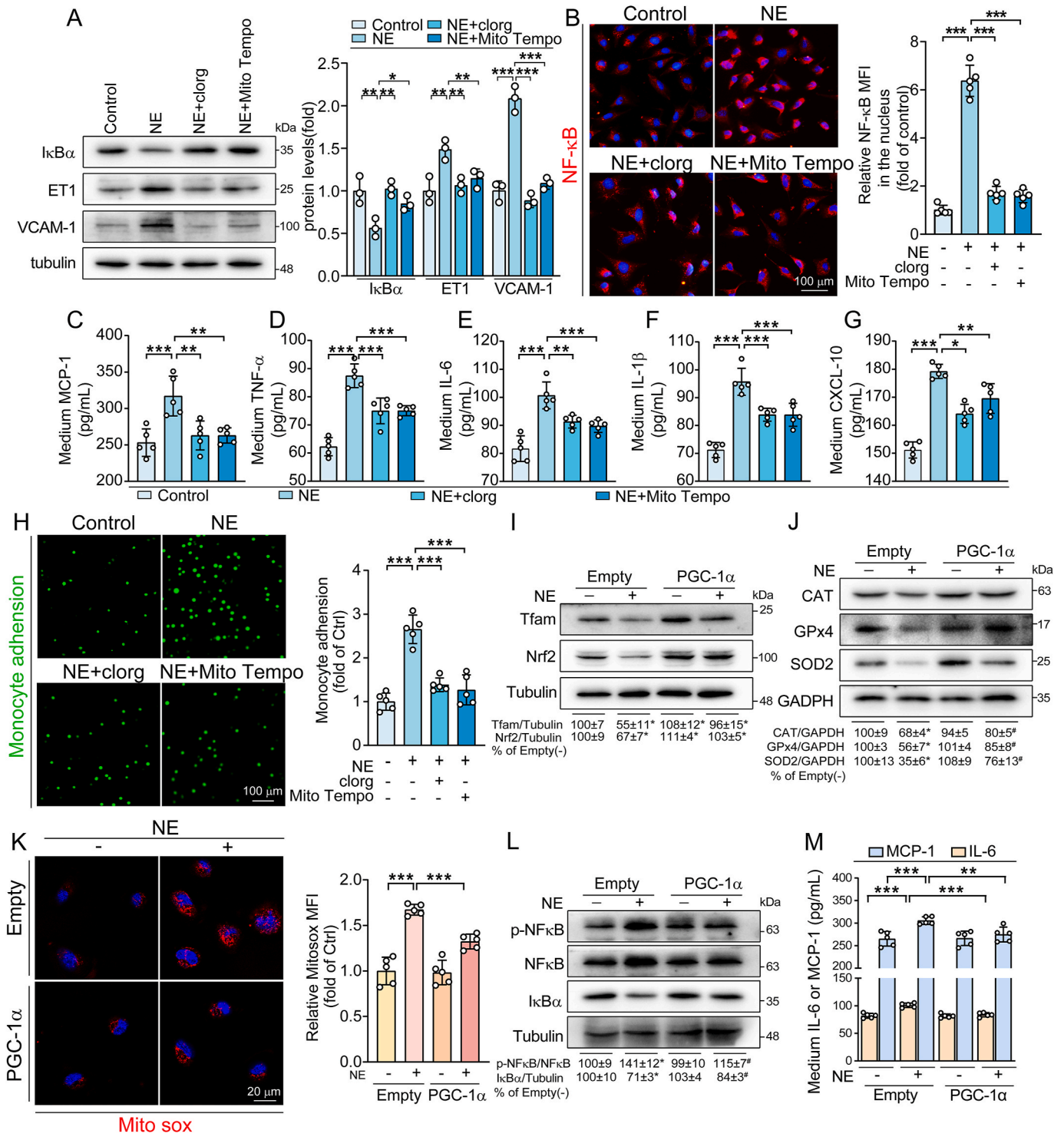

Fig. 6. MAO-A-induced mitochondrial ROS production facilitates NF-κB activation and production of proinflammatory cytokines in HAECs.
A–H: HAECs were treated with norepinephrine (NE, 10 μmol/L), NE plus clorgyline (clorg, 10 μmol/L), or NE plus MitoTempo (500 μmol/L) for 24 h. Cells and conditioned medium were collected for the following assays. Expression of IκB, ET-1 and VCAM-1 (**A**) by Western blot (n = 3); NF-κB p65 by immunofluorescent staining with quantification of MFI in the nucleus (**B**, n = 5). Levels of MCP-1, IL6, TNF-α, IL-1β, and CXCL10 (**C–G**) in conditioned medium by ELISA assay kits (n = 5). Adhesion of calcein-AM-labeled THP-1 monocytes to HAECs (**H**, n = 5). **I-M**: HAECs were transfected with empty or PGC-1α expression vector for 24 h, followed by norepinephrine (10 μmol/L) treatment for 24 h. Cells and conditioned medium were collected for the following assays. Expression of Tfam and Nrf2 (**I**), CAT, SOD2 and GPx4 (**J**), p-p65 and p65 of NF-κB and IκBα (**L**) by Western blot (n = 3); mitochondrial superoxide levels by MitoSOX Red staining with quantification of MFI (**K**, n = 5). Levels of MCP-1 and IL-6 in conditioned medium by ELISA assay kits (**M**) (n = 5). Data are presented as mean ± SD. *P < 0.05; **P < 0.01; ***P < 0.001 *vs.* Empty without NE treatment or as indicated, #P < 0.05 *vs.* Empty with NE treatment. ns: not significant. (For interpretation of the references to colour in this figure legend, the reader is referred to the Web version of this article.)

neurotransmitters and biogenic amines, including norepinephrine [14,38,39]. During this process, it generates more H_2O_2 with respect to mitochondrial respiratory chain [40], which is one of the major sources of ROS within mitochondria [14,41]. Under high levels of sympathetic tone, such as in cardiac failure and ischemia-reperfusion, circulating norepinephrine levels are elevated, leading to upregulation of MAO-A activity due to increased substrate availability [42]. In this study, we found that it is similar to norepinephrine, serum MAO-A levels were also significantly elevated in CAD patients (Fig. 1B) and ApoE$^{-/-}$ mice with atherosclerosis at advanced stage (Table S4). Reciprocally, associated with inhibition of atherosclerosis, RDN reduced MAO-A expression in tissue and serum MAO-A levels/activity in ApoE$^{-/-}$ mice (Fig. 1G, I, K, L; S1B). *In vitro*, treatment of HAECs with norepinephrine activated MAO-A expressions, which in turn promoted mitochondrial dysfunction and inflammatory responses that are associated with generation of mtROS (Fig. 5). However, all the impairment to mitochondria caused by norepinephrine were substantially attenuated by MAO-A inhibitors, clorgyline or siRNA (Fig. 5), suggesting the sympathetic hyperactivity-induced mitochondrial dysfunction is mediated through MAO-A activity.

PGC-1α plays a key role in EC regulation by exerting various effects on mitochondrial function, redox imbalance and inflammation [43–45]. PGC-1α activates several transcription factors, including Nrf2 and Tfam, to enhance expression of the molecules associated with mitochondrial biogenesis and anti-oxidative stress (SOD2, CAT and GPx) in ECs [46]. Moreover, PGC-1α and NF-κB are mutually regulated during inflammation and in the vicious cycle in which oxidative stress plays a vital role [47,48]. In this study, we found that in addition to suppressing endothelial inflammation, RDN also promoted expression of the molecules associated with mitochondrial biogenesis and antioxidant functions (Fig. 4), in line with PGC-1α effects. Furthermore, we found associated with inhibition of MAO-A expression, RDN activated PGC-1α expression in aortas (Figs. 1K and 4I). *In vitro*, norepinephrine-caused EC dysfunction/inflammation is mediated through activation of MAO-A (Fig. 5D–H), which were potently attenuated by activation of PGC-1α expression (Fig. 6; S4). These findings suggest the importance of PGC-1α in RDN-protected endothelial mitochondrial integrity, biogenesis and functions in the context of sympathetic hyperactivity.

A limitation of this study is that we only focused on the modulation of EC phenotypes by RDN during atherosclerosis progression. However, activation of sympathetic signaling is also able to modulate macrophage phenotypes and smooth muscle proliferation and migration [49,50]. Considering its roles in various pathologic conditions, sympathetic hyperactivity may promote different aspects of atherogenesis in advanced stages, including atheroma formation, progression, and rupture. The specific roles of RDN and MAO-A activity in various cell types during advanced atherosclerosis merits further investigation.

In conclusion, we elucidated the mechanisms underlying RDN-repaired endothelial dysfunctions during atherogenesis, which lays the foundation for the application of RDN in hypertensive patients complicated by atherosclerosis. Moreover, the finding that increased norepinephrine spillover regulates EC phenotypes *via* MAO-A mediated mitochondrial-inflammation circuit may provide very fruitful therapeutic targets for atherosclerosis treatment.

Funding

This study was supported by the National Natural Science Foundation of China (NSFC) grants 81970303 to C Lu and 81973316 to J Han.

Acknowledgements

We would like to thank Peng Zeng and Dan Zhao for technical assistance.

Appendix A. Supplementary data

Supplementary data to this article can be found online at https://doi.org/10.1016/j.redox.2021.102156.

Declaration of competing interest

All the authors declare that there are no conflicts of interest.

References

[1] G.A. Roth, M.H. Forouzanfar, A.E. Moran, R. Barber, G. Nguyen, V.L. Feigin, M. Naghavi, G.A. Mensah, C.J. Murray, Demographic and epidemiologic drivers of global cardiovascular mortality, N. Engl. J. Med. 372 (14) (2015) 1333–1341.
[2] P.M. Vanhoutte, Endothelial dysfunction: the first step toward coronary arteriosclerosis, Circ. J. 73 (4) (2009) 595–601.
[3] R.S. Balaban, S. Nemoto, T. Finkel, Mitochondria, oxidants, and aging, Cell 120 (4) (2005) 483–495.
[4] R. Sandhir, A. Halder, A. Sunkaria, Mitochondria as a centrally positioned hub in the innate immune response, Biochi Biophy Acta, Mol Basis Dis 1863 (5) (2017) 1090–1097.
[5] W. Cao, L. Wu, X. Zhang, J. Zhou, J. Wang, Z. Yang, H. Su, Y. Liu, C.S. Wilcox, F. F. Hou, Sympathetic overactivity in CKD disrupts buffering of neurotransmission by endothelium-derived hyperpolarizing factor and enhances vasoconstriction, J. Am. Soc. Nephrol. 31 (10) (2020) 2312–2325.
[6] J. Hinterdobler, S. Schott, H. Jin, A. Meesmann, A.L. Steinsiek, A.S. Zimmermann, J. Wobst, P. Müller, C. Mauersberger, B. Vilne, A. Baecklund, C.S. Chen, A. Moggio, Q. Braster, M. Molitor, M. Krane, W.E. Kempf, K.H. Ladwig, M. Hristov, M. Hulsmans, I. Hilgendorf, C. Weber, P. Wenzel, C. Scheiermann, L. Maegdefessel, O. Soehnlein, P. Libby, M. Nahrendorf, H. Schunkert, T. Kessler, H.B. Sager, Acute mental stress drives vascular inflammation and promotes plaque destabilization in mouse atherosclerosis, Eur. Heart J. (2021) 1–13, 00.
[7] M. Lee, R.A. Hemmes, J. Mynard, E. Lambert, G.A. Head, M. Cheung, I. E. Konstantinov, C.P. Brizard, G. Lambert, Y. D'Udekem, Elevated sympathetic activity, endothelial dysfunction, and late hypertension after repair of coarctation of the aorta, Int. J. Cardiol. 243 (2017) 185–190.
[8] A. de Juan, L.M. Ince, R. Pick, C.S. Chen, F. Molica, G. Zuchtriegel, C. Wang, D. Zhang, D. Druzd, M. Hessenauer, G. Pelli, I. Kolbe, H. Oster, C. Prophete, S. M. Hergenhan, U. Albrecht, J. Ripperger, E. Montanez, C.A. Reichel, O. Soehnlein, B.R. Kwak, P.S. Frenette, C. Scheiermann, Artery-associated sympathetic innervation drives rhythmic vascular inflammation of arteries and veins, Circulation 140 (13) (2019) 1100–1114.
[9] F.A. Santa-Rosa, G.L. Shimojo, D.S. Dias, A. Viana, F.C. Lanza, M.C. Irigoyen, K. De Angelis, Impact of an active lifestyle on heart rate variability and oxidative stress markers in offspring of hypertensives, Sci Rep-Uk 10 (1) (2020) 12439.
[10] I.T. Fonkoue, P.J. Marvar, S. Norrholm, Y. Li, M.L. Kankam, T.N. Jones, M. Vemulapalli, B. Rothbaum, J.D. Bremner, N.A. Le, J. Park, Symptom severity impacts sympathetic dysregulation and inflammation in post-traumatic stress disorder (PTSD), Brain Behav. Immun. 83 (2020) 260–269.
[11] H.B. Huan, X.D. Wen, X.J. Chen, L. Wu, L.L. Wu, L. Zhang, D.P. Yang, X. Zhang, P. Bie, C. Qian, F. Xia, Sympathetic nervous system promotes hepatocarcinogenesis by modulating inflammation through activation of alpha1-adrenergic receptors of Kupffer cells, Brain Behav. Immun. 59 (2017) 118–134.
[12] J. Mialet-Perez, Y. Santin, A. Parini, Monoamine oxidase-A, serotonin and norepinephrine: synergistic players in cardiac physiology and pathology, J. Neural. Transm. 125 (11) (2018) 1627–1634.
[13] S. Deshwal, M. Di Sante, F. Di Lisa, N. Kaludercic, Emerging role of monoamine oxidase as a therapeutic target for cardiovascular disease, Curr. Opin. Pharmacol. 33 (2017) 64–69.
[14] C. Villeneuve, C. Guilbeau-Frugier, P. Sicard, O. Lairez, C. Ordener, T. Duparc, D. De Paulis, B. Couderc, O. Spreux-Varoquaux, F. Tortosa, A. Garnier, C. Knauf, P. Valet, E. Borchi, C. Nediani, A. Gharib, M. Ovize, M.B. Delisle, A. Parini, J. Mialet-Perez, p53-PGC-1a pathway mediates oxidative mitochondrial damage and cardiomyocyte necrosis induced by monoamine oxidase-A upregulation: role in chronic left ventricular dysfunction in mice, Antioxidants Redox Signal. 18 (1) (2013) 5–18.
[15] M. Böhm, K. Kario, D.E. Kandzari, F. Mahfoud, M.A. Weber, R.E. Schmieder, K. Tsioufis, S. Pocock, D. Konstantinidis, J.W. Choi, C. East, D.P. Lee, A. Ma, S. Ewen, D.L. Cohen, R. Wilensky, C.M. Devireddy, J. Lea, A. Schmid, J. Weil, T. Agdirlioglu, D. Reedus, B.K. Jefferson, D. Reyes, R. D'Souza, A. Sharp, F. Sharif, M. Fahy, V. DeBruin, S.A. Cohen, S. Brar, R.R. Townsend, Efficacy of catheter-based renal denervation in the absence of antihypertensive medications (SPYRAL HTN-OFF MED Pivotal): a multicentre, randomised, sham-controlled trial, Lancet 395 (10234) (2020) 1444–1451.
[16] F. Mahfoud, G. Mancia, R. Schmieder, K. Narkiewicz, L. Ruilope, M. Schlaich, R. Whitbourn, A. Zirlik, T. Zeller, P. Stawowy, S.A. Cohen, M. Fahy, M. Böhm, Renal denervation in high-risk patients with hypertension, J. Am. Coll. Cardiol. 75 (23) (2020) 2879–2888.
[17] W. Cao, M. Shi, L. Wu, Z. Yang, X. Yang, H. Liu, X. Xu, Y. Liu, C.S. Wilcox, F.F. Hou, A renal-cerebral-peripheral sympathetic reflex mediates insulin resistance in chronic kidney disease, Ebiomedicine 37 (2018) 281–293.
[18] E.E. Nishi, N.R. Lopes, G.N. Gomes, J.C. Perry, A. Sato, M.G. Naffah-Mazzacoratti, C.T. Bergamaschi, R.R. Campos, Renal denervation reduces sympathetic

overactivation, brain oxidative stress, and renal injury in rats with renovascular hypertension independent of its effects on reducing blood pressure, Hypertens. Res. 42 (5) (2019) 628–640.
[19] Y. Wang, B. Rijal, M. Xu, Z. Li, Y. An, F. Zhang, C. Lu, Renal denervation improves vascular endothelial dysfunction by inducing autophagy via AMPK/mTOR signaling activation in a rat model of type 2 diabetes mellitus with insulin resistance, Acta Diabetol. 57 (10) (2020) 1227–1243.
[20] A. Daugherty, A.R. Tall, M. Daemen, E. Falk, E.A. Fisher, G. García-Cardeña, A. J. Lusis, A.P. Owens, M.E. Rosenfeld, R. Virmani, Recommendation on design, execution, and reporting of animal atherosclerosis studies: a scientific statement from the American heart association, Arterioscler. Thromb. Vasc. Biol. 37 (9) (2017) e131–e157.
[21] S. Zhang, F. Guo, M. Yu, X. Yang, Z. Yao, Q. Li, Z. Wei, K. Feng, P. Zeng, D. Zhao, X. Li, Y. Zhu, Q.R. Miao, Y. Iwakiri, Y. Chen, J. Han, Y. Duan, Reduced Nogo expression inhibits diet-induced metabolic disorders by regulating ChREBP and insulin activity, J. Hepatol. 73 (6) (2020) 1482–1495.
[22] K. Chauhan, J.M. Hernandez-Meza, A.G. Rodríguez-Hernández, K. Juarez-Moreno, P. Sengar, R. Vazquez-Duhalt, Multifunctionalized biocatalytic P22 nanoreactor for combinatory treatment of ER+ breast cancer, J. Nanobiotechnol. 16 (1) (2018) 17.
[23] A.J. Valente, L.A. Maddalena, E.L. Robb, F. Moradi, J.A. Stuart, A simple ImageJ macro tool for analyzing mitochondrial network morphology in mammalian cell culture, Acta Histochem. 119 (3) (2017) 315–326.
[24] B. Kennedy, M.G. Ziegler, A more sensitive and specific radioenzymatic assay for catecholamines, Life Sci. 47 (23) (1990) 2143–2153.
[25] H. Chen, R. Wang, F. Xu, T. Zang, M. Ji, J. Yin, J. Chen, L. Shen, J. Ge, Renal denervation mitigates atherosclerosis in ApoE-/- mice via the suppression of inflammation, Am. J. Transl. Res. 12 (9) (2020) 5362–5380.
[26] H. Wang, J. Wang, C. Guo, W. Luo, K. Kleiman, D.T. Eitzman, Renal denervation attenuates progression of atherosclerosis in apolipoprotein E-deficient mice independent of blood pressure lowering, Hypertension 65 (4) (2015) 758–765.
[27] Y. Wang, T.N. Dinh, A. Nield, S.M. Krishna, K. Denton, J. Golledge, Renal denervation promotes atherosclerosis in hypertensive apolipoprotein E-deficient mice infused with angiotensin II, Front. Physiol. 8 (2017) 215.
[28] R. Virmani, F.D. Kolodgie, A.P. Burke, A.V. Finn, H.K. Gold, T.N. Tulenko, S. P. Wrenn, J. Narula, Atherosclerotic plaque progression and vulnerability to rupture: angiogenesis as a source of intraplaque hemorrhage, Arterioscler. Thromb. Vasc. Biol. 25 (10) (2005) 2054–2061.
[29] C.K. Glass, J.L. Witztum, Atherosclerosis. the road ahead, Cell 104 (4) (2001) 503–516.
[30] N. Kaludercic, J. Mialet-Perez, N. Paolocci, A. Parini, F. Di Lisa, Monoamine oxidases as sources of oxidants in the heart, J. Mol. Cell. Cardiol. 73 (2014) 34–42.
[31] T. Suzuki, T. Hidaka, Y. Kumagai, M. Yamamoto, Environmental pollutants and the immune response, Nat. Immunol. 21 (12) (2020) 1486–1495.
[32] R.C. Scarpulla, Transcriptional paradigms in mammalian mitochondrial biogenesis and function, Physiol. Rev. 88 (2) (2008) 611–638.
[33] G. Grassi, G. Seravalle, G. Brambilla, G. Mancia, The sympathetic nervous system and new nonpharmacologic approaches to treating hypertension: a focus on renal denervation, Can. J. Cardiol. 28 (3) (2012) 311–317.
[34] M. Schlaich, N. Straznicky, E. Lambert, G. Lambert, Metabolic syndrome: a sympathetic disease? Lancet Diabetes Endocrinol. 3 (2) (2015) 148–157.
[36] M.A. Kluge, J.L. Fetterman, J.A. Vita, Mitochondria and endothelial function, Circ. Res. 112 (8) (2013) 1171–1188.
[37] E. Naik, V.M. Dixit, Mitochondrial reactive oxygen species drive proinflammatory cytokine production, J. Exp. Med. 208 (3) (2011) 417–420.
[38] M. Bortolato, K. Chen, J.C. Shih, Monoamine oxidase inactivation: from pathophysiology to therapeutics, Adv. Drug Deliv. Rev. 60 (2008) 1527–1533.
[39] Y. Santin, J. Resta, A. Parini, J. Mialet-Perez, Monoamine oxidases in age-associated diseases: new perspectives for old enzymes, Ageing Res. Rev. 66 (2021) 101256.
[40] E.J. Anderson, J.T. Efird, S.W. Davies, W.T. O'Neal, T.M. Darden, K.A. Thayne, L. A. Katunga, L.C. Kindell, T.B. Ferguson, C.A. Anderson, W.R. Chitwood, T. C. Koutlas, J.M. Williams, E. Rodriguez, A.P. Kypson, Monoamine oxidase is a major determinant of redox balance in human atrial myocardium and is associated with postoperative atrial fibrillation, J. Am. Heart Assoc. 3 (1) (2014), e000713.
[41] N. Hauptmann, J. Grimsby, J.C. Shih, E. Cadenas, The metabolism of tyramine by monoamine oxidase A/B causes oxidative damage to mitochondrial DNA, Arch. Biochem. Biophys. 335 (2) (1996) 295–304.
[42] N. Kaludercic, E. Takimoto, T. Nagayama, N. Feng, E.W. Lai, D. Bedja, K. Chen, K. L. Gabrielson, R.D. Blakely, J.C. Shih, K. Pacak, D.A. Kass, F. Di Lisa, N. Paolocci, Monoamine oxidase A-mediated enhanced catabolism of norepinephrine contributes to adverse remodeling and pump failure in hearts with pressure overload, Circ. Res. 106 (1) (2010) 193–202.
[43] A.O. Kadlec, D.S. Chabowski, K. Ait-Aissa, D.D. Gutterman, Role of PGC-1α in vascular regulation: implications for atherosclerosis, Arterioscler. Thromb. Vasc. Biol. 36 (8) (2016) 1467–1474.
[44] I. Valle, A. Alvarez-Barrientos, E. Arza, S. Lamas, M. Monsalve, PGC-1alpha regulates the mitochondrial antioxidant defense system in vascular endothelial cells, Cardiovasc. Res. 66 (3) (2005) 562–573.
[45] S. Rius-Pérez, I. Torres-Cuevas, I. Millán, Á.L. Ortega, S. Pérez, PGC-1α, Inflammation, and oxidative stress: an integrative view in metabolism, Oxid. Med. Cell. Longev. 2020 (2020) 1452696.
[46] J.S. Bhatti, G.K. Bhatti, P.H. Reddy, Mitochondrial dysfunction and oxidative stress in metabolic disorders - a step towards mitochondria based therapeutic strategies, Biochim. Biophys. Acta (BBA) - Mol. Basis Dis. 1863 (5) (2017) 1066–1077.
[47] P.S. Eisele, C. Handschin, Functional crosstalk of PGC-1 coactivators and inflammation in skeletal muscle pathophysiology, Semin. Immunopathol. 36 (1) (2014) 27–53.
[48] D. Alvarez-Guardia, X. Palomer, T. Coll, M.M. Davidson, T.O. Chan, A.M. Feldman, J.C. Laguna, M. Vázquez-Carrera, The p65 subunit of NF-kappaB binds to PGC-1alpha, linking inflammation and metabolic disturbances in cardiac cells, Cardiovasc. Res. 87 (3) (2010) 449–458.
[49] J. Lyu, M. Wang, X. Kang, H. Xu, Z. Cao, T. Yu, K. Huang, J. Wu, X. Wei, Q. Lei, Macrophage-mediated regulation of catecholamines in sympathetic neural remodeling after myocardial infarction, Basic Res. Cardiol. 115 (5) (2020) 56.
[50] R.M. Touyz, R. Alves-Lopes, F.J. Rios, L.L. Camargo, A. Anagnostopoulou, A. Arner, A.C. Montezano, Vascular smooth muscle contraction in hypertension, Cardiovasc. Res. 114 (4) (2018) 529–539.